Contents list available at CBIORE journal website

International Journal of Renewable Energy Development

Journal homepage: https://ijred.cbiore.id

Research Article

Facile one-step hydrothermal carbonization of coffee husks into activated hydrochar for efficient methylene blue adsorption: Isotherm and kinetic studies

Thi Hien Tran*

Institute of Environmental Science, Engineering and Management, Industrial University of Ho Chi Minh City, 12 Nguyen Van Bao, Hanh Thong Ward, Ho Chi Minh City 700000, Vietnam

Abstract. Recycling agricultural waste into high-performance adsorbent materials represents a sustainable approach for environmentally friendly wastewater treatment, reflecting an important strategy for resource valorization. This study presents an accelerated and simplified route for synthesizing activated hydrochar (AHC) from coffee husks, an abundant lignocellulosic residue. The synthesis employs a one-step hydrothermal carbonization (HTC) under mild conditions (130 °C, 2 h) using 1 mol/L KOH as the activating reagent, followed by pyrolysis. By integrating carbonization and chemical activation into a single HTC stage, the process eliminates the conventional preliminary hydrochar-forming step. It thereby achieves substantial reductions in reaction time and energy input compared with conventional two-stage HTC methods. The resulting AHC exhibits a highly developed microporous architecture, with a BET surface area of 1022.34 m^2/g and a surface functionality density of 1.803 mmol/g, both of which contribute to enhanced adsorption performance. Methylene blue adsorption experiments reveal a maximum experimental capacity of 477.43 mg/g, in agreement with the Langmuir monolayer model (Q_m = 499.48 mg/g). Kinetic evaluation demonstrates excellent conformity with the pseudo-second-order rate law (R^2 = 0.9999), indicating rapid and surface-controlled adsorption. The material also retains stable adsorption efficiency over five consecutive regeneration cycles, confirming its robustness and reusability. Collectively, these findings demonstrate that coffee husks constitute a promising precursor for developing efficient adsorbents through a simple, accessible, and energy-efficient one-step HTC strategy. This work provides a practical and sustainable pathway for the valorization of agricultural residues while addressing critical challenges associated with the scalable remediation of dye-contaminated aqueous systems.

Keywords: Hydrothermal carbonization, Activated Hydrochar, Coffee husk, Adsorption kinetics

Received:15th Oct 2025; Revised: 18th Nov 2025; Accepted: 10th Dec 2025; Available online: 28th Dec 2025

1. Introduction

In 2024, the global production of synthetic dyes and organic pigments was estimated to reach approximately 5.3 million metric tons (Indexbox, 2024). The Asia–Pacific region accounted for the majority of this output, contributing nearly 51% of the total volume (around 2.7 million tons). Among the leading producers, China ranked first with an estimated output volume of 1.4 million tons, followed by Turkey (approximately 889 thousand tons) and India (around 863 thousand tons) (Indexbox, 2024). Despite their industrial significance, the uncontrolled discharge of synthetic dyes into aquatic ecosystems has raised serious environmental concerns, primarily due to their potential toxicity to aquatic life and associated health risks to humans. This is attributed to the inherent chemical stability, low biodegradability, and persistent toxicity of these compounds. Methylene blue (MB), widely employed as a model cationic chromophore in dye-related studies, is a prevalent contaminant in wastewater streams from textile manufacturing and poses significant risks to both aquatic life and human well-being at trace levels (Tran *et al.* (2020).

Among the available techniques for dye removal, adsorption is widely regarded as one of the most viable and efficient methods, owing to its technical simplicity, excellent pollutant removal capability, and low operational cost (Rocha *et al.*, 2020). Among various adsorbents, activated carbon has long been regarded as the reference standard, owing to its extensive surface area, highly organized pore network, rich surface functionalities, and superior chemical stability (Gil-Muñoz *et al.*, 2025). Typically, activated carbon is produced from renewable biomass precursors such as corncob (Selvam *et al.*, 2021), flax fibre (Illingworth *et al.*, 2022), rice husk (Nandi *et al.*, 2023), crab shell waste (Yang *et al.*, 2024), brewer's spent grain-based (Liu *et al.*, 2024), rubber seed shell (Rustamaji *et al.*, 2025), Napier grass, rubber wood, bamboo (Khruengsai *et al.*, 2024) and oak fruits (Akbari *et al.*, 2025) via a two-step process. Initially, the precursor undergoes thermal decomposition between 400 and 800 °C, yielding a carbon-rich intermediate known as char. This is followed by a chemical or physical activation stage conducted at higher temperatures (600 – 1000 °C), which facilitates the development of porous networks and enhances adsorption capacity (Medhat *et al.*, 2021, Illingworth *et al.*, 2022, Nandi *et al.*, 2023, Liu *et al.*, 2024) . However, this conventional method involves multiple processing stages, is energy-intensive, and requires technically sophisticated equipment. In particular,

* Corresponding author
Email: tranthihien@iuh.edu.vn (T. H. Tran)

https://doi.org/10.61435/ijred.2026.61885
ISSN: 2252-4940/© 2026.The Author(s). Published by CBIORE

microwave-assisted activation often leads to localized overheating, which may degrade the structural integrity of the adsorbent and reduce its overall adsorption performance (Polaert *et al.*, 2010).

Against this backdrop, hydrothermal carbonization (HTC) has gained considerable attention as a sustainable thermochemical pathway for valorizing wet biomass, owing to its moderate reaction conditions and reduced environmental footprint (Selvaraj *et al.*, 2025). The HTC process is conducted in an aqueous medium under autogenous pressure at relatively low temperatures (160 – 250 °C), allowing direct conversion of moisture-containing biomass into carbonaceous solids without requiring a preliminary drying stage (Tran *et al.*, 2016). This not only reduces the risk of fire or explosion but also contributes to overall energy savings (Tran *et al.*, 2022). Recent studies have applied HTC for the synthesis of hydrochar, a carbonaceous material characterized by a developed microporous structure, high abundance of oxygen-containing functional groups, and considerable potential for wastewater treatment applications (Selvaraj *et al.*, 2025). Hydrochar can be further activated using chemical agents (e.g., KOH, H_3PO_4, $ZnCl_2$), physical methods (e.g., steam, CO_2), or a combination involving post-pyrolysis to enhance its adsorption performance (Tran *et al.*, 2020, Tran *et al.*, 2021, Jalilian *et al.*, 2024, Rustamaji *et al.*, 2022, Hendronursito *et al.*, 2025). Notably, Luo *et al.* (2024) proposed a one-step HTC approach using hydrochloric acid to directly activate rice husk at 180 °C, resulting in an efficient adsorbent for the removal of levofloxacin.

Within the coffee value chain, coffee husk is the primary by-product generated during post-harvest processing, accounting for approximately 12 – 18% of the dry coffee cherry weight and amounting to nearly 10 million tons annually worldwide (Tamilselvan *et al.*, 2024). According to the United States Department of Agriculture (USDA), global green coffee production for the 2024/25 crop year is projected to reach 174.4 million bags (60 kg/ bag), equivalent to over 10.4 million metric tons, with Vietnam and Brazil being the leading producers (Service, 2025). Vietnam's output is estimated at 30.1 million bags, exceeding earlier forecasts (29 million bags), indicating a capacity for stable production despite challenges related to climate change and rising input costs (Rubinstein, 2024, Service, 2025). In Vietnam, a substantial portion of coffee husks remains underutilized and is commonly managed through unsustainable practices, thereby contributing to environmental pollution. Due to its high lignocellulosic content and favorable decomposition behavior under hydrothermal conditions, coffee husk is regarded as an attractive biomass precursor for the production of functional carbonaceous materials (Tran *et al.*, 2016, De Benedicto *et al.*, 2024). This process yields hydrochar and activated carbon with strong potential for wastewater remediation and the management of organic pollutants (Tran *et al.*, 2017, Krishna Murthy *et al.*, 2020, Tran *et al.*, 2020, Tran *et al.*, 2021). Valorizing this agricultural residue into high-performance adsorbents not only enables more sustainable waste management but also aligns with the broader goals of green materials development and circular economy strategies in both the agricultural and bio-based industrial sectors.

Following the trend of bio-based adsorbents, this study proposes a straightforward synthesis method that combines hydrothermal carbonization and chemical activation into a single step to produce activated hydrochar (AHC) from coffee husks, using KOH as the activating agent under mild conditions (130 °C, 2 h). This integrated process eliminates the need for separate treatment stages, thereby reducing processing time, lowering energy consumption, and minimizing operational costs. The synthesized AHC possesses an extensively developed pore network, elevated specific surface area, and abundant reactive surface functionalities, collectively enhancing its capability for MB removal from wastewater. Batch adsorption experiments demonstrated that AHC can rapidly and effectively remove MB, while maintaining stable performance over multiple regeneration cycles. This study presents an eco-friendly and feasible approach for valorizing agricultural residues in the treatment of contaminated water.

2. Methods and Materials

2.1 Raw material

Coffee husks derived from *Coffea canephora* (*Robusta variety*) were sourced from a post-harvest processing facility located in Dak Lak Province, Vietnam (Tran *et al.*, 2020). The raw coffee husk was mechanically ground and screened to achieve particles within the 250–500 µm range, which were subsequently used in the subsequent treatment procedures (see Fig. 1).

2.2 Adsorbate

Methylene blue, a basic dye widely employed as a model contaminant, was purchased from Xilong Chemical Co., Ltd. China (see Fig. 2) (Tran *et al.*, 2021). MB solutions at the required concentrations were prepared using ultrapure distilled water produced by a two-stage distillation system (Model A4000D, Bibby Instruments, UK), ensuring the elimination of background interference during adsorption experiments and spectrophotometric analysis.

2.3. Preparation of Activated Hydrochar (AHC)

For synthesis, 10 g of coffee husks was dispersed in 200 mL of KOH solution at concentrations (0.1, 0.25, 0.5, 1, and 2 mol/L). The suspension was magnetically stirred for 30 min, transferred into a 400 mL Teflon-lined stainless-steel autoclave (Tran *et al.*, 2020). The HTC was conducted at temperatures ranging from 110 to 170 °C (in 20 °C increments), for residence times of 0.5, 1, 2, 3, and 4 hours. The resulting hydrothermal solids were recovered by filtration without washing, dried at 105 °C, and

Fig 1. Coffee husk was milled and screened to achieve a uniform size of < 500 µm

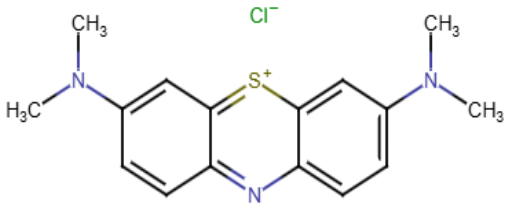

Fig 2. Molecular structure of MB dye.

subsequently pyrolyzed at 700 °C for 2 h under a continuous N_2 atmosphere in a tubular furnace (Wei *et al.*, 2015, Tran *et al.*, 2021). The pyrolyzed products were sequentially washed with dilute HCl and deionized water until neutral pH was achieved, followed by drying at 105 °C to yield the activated hydrochar (AHC) (Wei *et al.*, 2015, Tran *et al.*, 2020, Tran *et al.*, 2021, Tran *et al.*, 2022). The effects of KOH concentration, carbonization temperature, and residence time were systematically evaluated by measuring the MB adsorption capacity of the obtained samples to identify the optimal synthesis conditions (Tran *et al.*, 2022).

The physicochemical characteristics of AHC were comprehensively analyzed using several instrumental techniques. Surface morphology was examined using a scanning electron microscope (Hitachi S-4800, Japan). Textural parameters, including specific surface area and pore size distribution, were determined by nitrogen adsorption–desorption measurements using a Quantachrome Nova 1000E analyzer (USA) (Tran *et al.*, 2020). Surface functional groups were determined by Fourier-transform infrared (FTIR) spectroscopy (Bruker Tensor 27, Germany). The quantification of surface functionalities on the AHC sample was conducted using a Boehm titration with a potentiometric Metrohm Titrino Plus titrator (Tran *et al.*, 2020).

2.4 Adsorption equilibrium and kinetic investigations

2.4.1 Adsorption Equilibrium Studies

To evaluate the MB adsorption performance of the AHC material, a series of batch experiments was carried out. Each test involved beakers filled with 300 mL of MB solutions prepared at varying initial concentrations (50, 100, 200, 300, 400, and 500 mg/L) and the pH of the solutions (pH =7) (Tran *et al.*, 2020). The adsorbent was applied at a fixed dosage of 1 g/L across all samples. After equilibration, all suspensions were centrifuged to remove particulates, thereby avoiding interference from residual solids in subsequent measurements. The concentrations of MB before and after the adsorption process were determined at λ_{max} 665 nm using a GENESYS 10S UV-Vis spectrometer (Tran *et al.*, 2020). Control samples were prepared in parallel using identical MB solutions without the presence of adsorbent to account for potential non-adsorptive losses. The determination of adsorption capacity was performed based on the standard adsorption models described in Eq.1 (Tran *et al.*, 2022, Hussein *et al.*, 2026).

$$q_e = \frac{(C_o - C_e)V}{W} \quad (1)$$

Where: C_o, C_e (mg/L) denote the initial and equilibrium MB concentrations onto AHC, W (g) is the weight of AHC adsorbent, V (L) denotes the total solution volume of MB.

A sequence of controlled adsorption trials was carried out to determine the optimum operational parameters governing methylene blue removal by AHC. Experimental variables were systematically adjusted, including solution pH (3 – 11), agitation rate (0 – 400 rpm), adsorbent loading (0.25 – 2.0 g/L), and contact duration (up to 180 min), while the starting MB concentration was maintained at 100 mg/L throughout the experiments.

The removal efficiency of MB was evaluated using Eq. 2:

$$\text{Remove MB yield } \% = \frac{(C_o - C_t)}{C_o} \times 100 \quad (2)$$

Where: C_t (mg/L) is the MB concentration at time t

2.4.2 Adsorption Isotherm Modeling

The Langmuir isotherm postulates that adsorption takes place as a single molecular layer on a uniform surface possessing a limited number of energetically identical active sites, with no lateral interactions among the adsorbed species. The Langmuir equation is given as (Tran *et al.*, 2020, Tran *et al.*, 2022):

$$\frac{C_e}{q_e} = \frac{C_e}{Q_m} + \frac{1}{Q_m.K_L} \quad (3)$$

Where: q_e (mg/g) is the equilibrium adsorption capacity, C_e (mg/L) is the equilibrium concentration of the adsorbate, Q_m (mg/g) is the theoretical maximum monolayer adsorption capacity, K_L (L/mg) is the Langmuir equilibrium constant.

In addition, the applicability of the Langmuir isotherm was further assessed using the dimensionless separation factor (R_L) presented in Table 2, which is calculated according to Eq.4 (Tran *et al.*, 2022).

$$R_L = \frac{1}{1 + K_L C_o} \quad (4)$$

Where: C_o (mg/L) is initial MB concentration, K_L (L/mg) is the Langmuir constant.

The Freundlich isotherm was utilized to assess the potential of multilayer adsorption on heterogeneous surfaces of the activated hydrochar. The Freundlich model is an empirical equation suited for adsorption processes on heterogeneous surfaces, where multilayer adsorption can occur and binding site energies vary. The Freundlich equation is expressed as (Tran *et al.*, 2020, Tran *et al.*, 2022):

$$log\, q_e = log\ K_F + \frac{1}{n} log\ C_e \quad (5)$$

Where: q_e (mg/g) and C_e (mg/L) are the equilibrium adsorption capacity and solute concentration, respectively, K_F [(mg/g)(L/mg)$^{1/n}$] is the Freundlich constant indicative of adsorption capacity, n is the intensity parameter reflecting adsorption favorability.

2.4.3 Kinetics of adsorption

The kinetic characteristics of MB adsorption onto AHC were examined through time-resolved batch experiments performed under the same operational parameters as in the equilibrium assays. At predetermined intervals, solution samples were collected to track variations in MB concentration. The adsorption capacity at a given time, q_t (mg/g), was calculated using Eq. 6, allowing for the assessment of adsorption kinetics and the underlying mechanism throughout the experimental period (Tran *et al.*, 2020, Tran *et al.*, 2022).

$$q_t = \frac{(C_o - C_t)V}{W} \quad (6)$$

Where: C_o, C_t (mg/L) represent the initial and at a time t of MB onto AHC, W (g) is the weight of AHC adsorbent, V (L) denotes the total solution volume of MB.

To elucidate the adsorption kinetics of MB on AHC, the time-dependent behavior was analyzed using two conventional kinetic models: pseudo-first-order (PFO) and pseudo-second-order (PSO) equations. The PFO model follows Lagergren's expression (Eq. 7) (Tran *et al.*, 2020, Tran *et al.*, 2022):

$$\ln (q_e - q_t) = \ln q_e - k_1 t \quad (7)$$

Where: q_e equilibrium capacity, q_t capacity at time t, and k_1 is the rate constant.

The PSO model (Eq. 8) assumes that the adsorption rate is governed by chemical interactions and is given by:

$$\frac{t}{q_t} = \frac{1}{k_2 q_e^2} + \frac{t}{q_e} \quad (8)$$

with k_2 [g/(mg.min)] as the rate constant and the initial adsorption rate (h) calculated using Eq.9 (Tran *et al.*, 2022).

$$h = k_2 \times q_e^2 \quad (9)$$

The best-fitting kinetic and isotherm parameters were determined by minimizing the residual sum of squares (Eq. 10):

$$SSE(\%) = \sqrt{\frac{\sum \left(q_{e,exp} - q_{e,cal}\right)^2}{N}} \quad (10)$$

Where: N is the number of data points for MB adsorption (Tran *et al.*, 2022).

3. Results and discussion

3.1. Preparation of activated hydrochar

3.1.1. Effect of KOH activation concentration on the development of surface acidity and adsorption performance of AHC

As shown in Figure 3, the concentration of KOH used during the hydrothermal activation process had a pronounced influence on both the surface acidity and the MB adsorption capacity of AHC. A progressive increase in KOH concentration from 0.1 to 1 mol/L resulted in a pronounced elevation of the total surface acidity of AHC, which rose from 0.390 to 1.797 mmol/g with the variation being statistically significant ($p < 0.05$). This can be attributed to the strong oxidizing nature of KOH, which promotes the formation of oxygen-containing functional groups on the carbon surface, such as carboxylic (-COOH), phenolic (-OH), carbonyl (=CO), and lactonic groups (Tran *et al.*, 2022, Liu *et al.*, 2024). These acidic surface functionalities substantially contribute to the overall surface acidity of the activated hydrochars (Tran *et al.*, 2020, Liu *et al.*, 2024). In addition to the formation of new oxygenated moieties, the enhancement in surface acidity may also stem from structural rearrangements within the carbon framework induced by alkaline activation. The reaction of KOH with amorphous carbon domains generates more defect and edge sites, thereby exposing reactive positions that can subsequently anchor oxygen functionalities. Such microstructural evolution enhances the accessibility and density of acid–base active centers, reinforcing the measured total surface acidity and facilitating the adsorption of cationic species.

A corresponding increase in MB removal efficiency was also observed from 40.98% to 99.39% as the KOH concentration increased from 0.1 to 1 mol/L. This enhancement is likely due to the increased density of acidic functional groups on AHC's surface, which facilitates greater interaction with cationic dye molecules (Saha *et al.*, 2020). However, once the activation medium exceeded 1 mol/L KOH, the adsorption performance tended to plateau, suggesting a saturation of reactive sites and partial structural densification. At excessive alkali concentrations, over-etching and local pore collapse can occur, removing fragile surface groups and reducing accessible microporosity. Consequently, the number of effective adsorption sites remains nearly constant beyond this concentration, leading to only marginal improvements in surface acidity and MB adsorption.

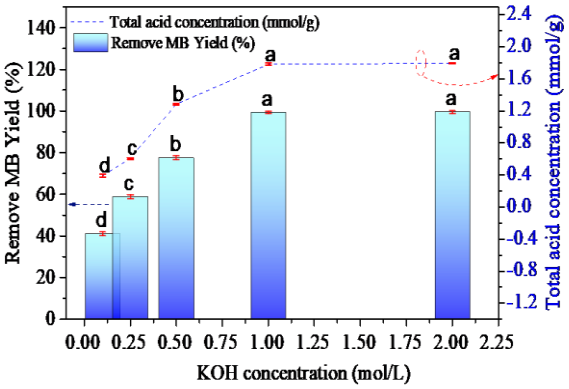

Fig 3. Influence of KOH concentration during hydrothermal carbonization on MB adsorption capacity; different letters indicate significance (Tukey HSD, $p < 0.05$).

Further increasing the KOH concentration from 1 to 2 mol/L resulted in only a marginal change in total acidity (Δ = 0.008 mmol/g, $p < 0.05$) and MB adsorption (Δ = 0.15%). Statistical analysis using Tukey's test confirmed the absence of a significant difference between the adsorption performances at 1 and 2 mol/L KOH, as both were grouped under the same statistical category. Therefore, a KOH concentration of 1 mol/L can be regarded as optimal for producing activated hydrochar with high MB adsorption capacity, in agreement with previous studies (Wei *et al.*, 2015, Tran *et al.*, 2020, Tran *et al.*, 2021).

3.1.2. Effect of hydrothermal carbonization temperature.

The impact of HTC temperature on the MB adsorption performance of AHC is illustrated in Figure 4. As shown in Fig. 4, the HTC temperature had a pronounced effect on the MB adsorption efficiency of AHC. When the HTC temperature increased from 110 °C to 150 °C, the MB removal efficiency rose significantly from 56.61% to 99.17% ($p < 0.05$). This improvement was accompanied by an increase in the total surface acidity, which grew from 0.594 to 1.768 mmol/g. The remarkable enhancement in MB adsorption efficiency within this temperature range likely arises from a synergistic effect between chemical activation and microstructural evolution. As the HTC temperature increases, dehydration and decarboxylation reactions intensify, leading to partial aromatization of the carbon skeleton and concurrent formation of oxygenated functional groups (Gong *et al.*, 2025). This dual mechanism simultaneously increases the density of active sites and enhances pore accessibility, both of which contribute to higher dye adsorption capacity.

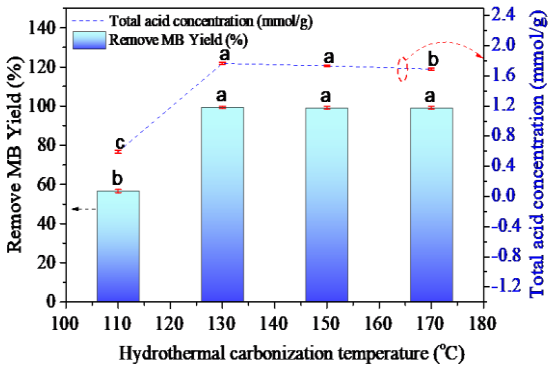

Fig 4. Impact of HTC temperature on MB adsorption efficiency; different letters indicate significance (Tukey HSD, $p < 0.05$).

However, a further increase in HTC temperature from 150 °C to 170 °C resulted in a slight decrease in adsorption performance, with MB removal efficiency dropping from 99.41% to 99.16% ($p < 0.05$). This decline correlated with a reduction in total acidity from 1.768 to 1.692 mmol/g, likely due to thermal degradation of surface oxygen-containing functional groups at elevated temperatures. These findings are consistent with Tukey's HSD test, which indicated no statistically significant difference between samples treated at 150 °C and 170 °C. Based on adsorption performance and energy considerations, 130 °C was identified as the optimal HTC temperature for AHC preparation. These results are consistent with previous findings (Wei *et al.*, 2015, Tran *et al.*, 2020, Tran *et al.*, 2021).

3.1.3. Effect of Hydrothermal Carbonization Time

The influence of HTC time on the MB adsorption capacity of AHC is illustrated in Figure 5**.** As shown in Figure 5, the duration of HTC exerts a significant influence on the MB adsorption capacity of AHC, highlighting the time-dependent behavior of the material's adsorption performance. As the HTC time increased from 0.5 to 4 hours, the MB removal efficiency improved from 54.51% to 98.01% ($p < 0.05$), accompanied by a corresponding increase in total surface acidity from 0.399 to 1.803 mmol/g. However, further extension of the HTC time to 4 hours led to a slight decline in removal efficiency (down to 98.01%), likely attributed to the degradation of surface functional groups during prolonged hydrothermal treatment, which in turn lowers the surface acidity and adsorption capacity. The trends observed were statistically validated through Tukey's Honestly Significant Difference (HSD) analysis. Therefore, an HTC duration of 2 hours is identified as the optimal condition for producing AHC with superior MB adsorption performance, aligning with earlier research findings (Wei *et al.*, 2015).

In summary, the most favorable condition for the synthesis of AHC with superior MB dye adsorption was determined to be 1 mol/L KOH at 130 °C for 2 h. These conditions not only ensure effective adsorption capacity but also provide practical advantages, such as reducing chemical consumption and simplifying the synthesis process. Notably, the residual KOH remaining after hydrothermal processing still participates in the subsequent thermal treatment, effectively integrating chemical activation with thermal processing. This integrated strategy offers a promising solution to overcome the low carbon yield limitations commonly associated with direct pyrolysis of lignocellulosic biomass (Bielecki *et al.*, 2023, Jerzak *et al.*, 2024).

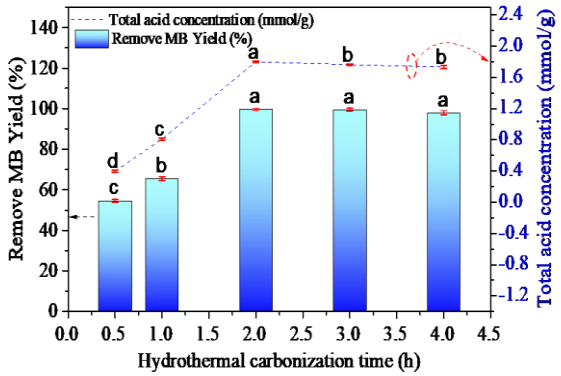

Fig 5. Impact of HTC time on MB adsorption, different letters indicate significance (Tukey HSD, $p < 0.05$).

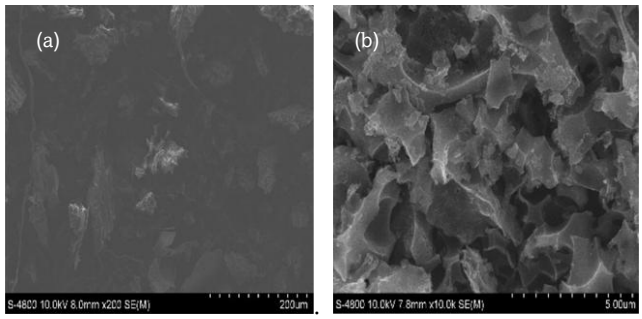

Fig 6. SEM images of (a) raw coffee husk and (b) AHC

3.2. Characterization of AHC

The surface morphology and structural characteristics of the AHC were examined using scanning electron microscopy (SEM), as shown in Figure 6. The SEM image of the raw coffee husk (Fig.6a) reveals a compact and rigid surface with a limited number of visible pores. In contrast, the surface morphology of the AHC (Fig.6b) demonstrates significant structural transformation following hydrothermal carbonization in the presence of KOH. The resulting AHC exhibits a loose, layered structure with an irregular pore distribution and non-uniform pore sizes, indicating the development of a more porous texture as a result of chemical activation.

These results are consistent with the specific surface area and pore characteristics of the AHC. The material showed a large BET surface area of 1022.34 m^2/g. The nitrogen adsorption–desorption isotherms shown in Figure 7a display a hybrid profile between type I and type IV according to the IUPAC classification, indicating the coexistence of micropores and mesopores (Tran *et al.*, 2020). The pore size distribution curve (Fig.7b), obtained using the Dubinin–Astakhov (DA) micropore model, reveals an average pore diameter of approximately 15.6 Å, further confirming the hierarchical porous structure.

The high porosity and enlarged surface area are primarily attributed to the removal of organic compounds during the HTC of coffee husk in the presence of KOH. Under hydrothermal conditions with elevated autogenous pressure, KOH interacts with the polyaromatic structure of hydrochar, facilitating the elimination of volatile species and enhancing the development

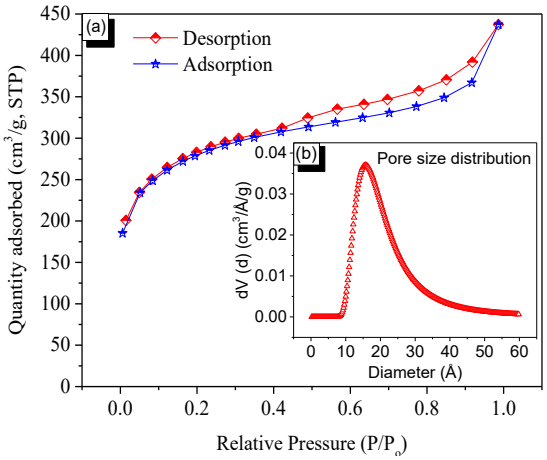

Fig 7. The nitrogen adsorption–desorption isotherms (a) and the corresponding pore size distribution (b) of the AHC.

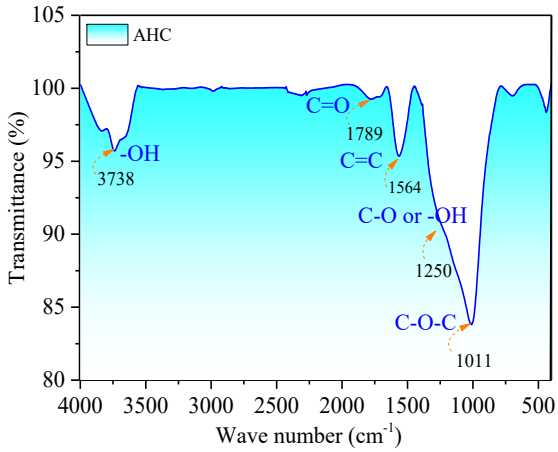

Fig 8. FTIR spectra of the activated hydrochar.

of hydrophilic functional groups such as carboxylic and phenolic moieties. This structural evolution significantly contributes to the increased adsorption potential of the AHC.

The FTIR spectrum of AHC (Fig. 8) exhibits a prominent absorption peak at 3416 cm^{-1}, which corresponds to the characteristic O–H stretching vibrations typically associated with hydroxyl groups present in carboxylic acids or phenolic moieties originating from the lignin and cellulose components of the precursor biomass. This observation indicates the presence of "free" hydroxyl groups on the surface of the activated hydrochar (Tran *et al.*, 2020, Pathania *et al.*, 2017, Tran *et al.*, 2021). A distinct band at 1780 cm^{-1} is attributed to the C=O stretching vibrations of carbonyl-containing functional groups, such as anhydrides, carboxylic acids, or esters. The presence of C=O groups suggests that the surface of the hydrochar incorporates oxygen-containing functionalities, which are likely to enhance its adsorption performance through increased hydrophilicity and the ability to form hydrogen bonds with polar organic pollutants, including synthetic dyes. The absorption band observed at 1564 cm^{-1} falls within the range characteristic of aromatic C=C stretching, implying the formation of aromatic ring structures in the carbon structures. The presence of such structures is indicative of a high degree of aromatic rings in the hydrochar, a feature that is often linked to enhanced adsorption capabilities. Furthermore, a broad absorption band spanning from 1000 to 1200 cm^{-1}, with a maximum at 1010 cm^{-1}, is assigned to C–O stretching vibrations. These are associated with primary alcohol groups or residual polysaccharide structures derived from the original biomass. The FTIR characteristics of the AHC obtained are consistent with those previously reported for adsorbents derived from coffee husks (Tran *et al.*, 2021, Tran *et al.*, 2022).

Table 1 summarizes the numerical assessment of the chemical functionalities present on AHC, as identified through Boehm titration analysis (Tran *et al.*, 2022). The enhanced abundance of oxygen-containing functionalities induced by KOH-assisted hydrothermal activation is regarded as a key determinant influencing the methylene blue adsorption performance (Tran *et al.*, 2022, Tran *et al.*, 2021, Jain *et al.*, 2016). Boehm titration data (Table 1) reveal substantial differences in the surface oxygenated functional group contents between the activated hydrochar (AHC-KOH 1M) prepared via the conventional two-step hydrothermal carbonization–pyrolysis route (Tran *et al.*, 2021) and the one-step hydrothermal carbonization–KOH activation approach used in this study. While both methods produced materials with a high abundance of surface functionalities, the two-step AHC-KOH 1M exhibited a slightly higher total oxygenated group content (1.873 mmol/g) compared to the one-step AHC (1.803 mmol/g). Notably, the one-step AHC possessed a markedly higher lactonic group content (0.543 mmol/g vs. 0.415 mmol/g), whereas the two-step AHC-KOH 1M contained greater amounts of carboxylic (0.868 mmol/g) and phenolic groups (0.590 mmol/g). These variations can be attributed to differences in thermal history and activation mechanisms. In the two-step process, the intermediate hydrochar undergoes a separate pyrolysis stage at elevated temperatures, which promotes partial decomposition of lactones into more thermally stable carboxylic and phenolic moieties through oxidative surface transformations. In contrast, the one-step HTC–KOH activation conducted under milder hydrothermal conditions facilitates nucleophilic attack of hydroxide ions on carbonaceous structures, leading to preferential formation and stabilization of lactonic functionalities while limiting excessive decarboxylation and phenol condensation. Furthermore, the shorter reaction time and lower thermal stress in the one-step method help preserve certain oxygenated species that are otherwise degraded in high-temperature pyrolysis.

Table 1
Surface functional group content of AHC determined by Boehm titration

Oxygenated functional groups (mmol/g)	Raw Hydrochar (Tran *et al.*, 2021)	AHC-KOH 1M (Tran *et al.*, 2021)	AHC this study
Carboxylic (-COOH)	0.064	0.868	0.768
Lactones (-CO)	0.097	0.415	0.543
Phenolics (-OH)	0.307	0.590	0.492
Total	0.468	1.873	1.803

3.3. Adsorption performance of MB onto AHC

3.3.1. Influence of operational parameters on MB adsorption by AHC

a. Effect of stirring speed on adsorption

The influence of stirring speed on the adsorption performance of AHC toward MB was examined in the range of 0 to 400 rpm under constant experimental conditions: initial MB 100 mg/L, 30°C, 180 min, as shown in Fig. 9. A significant improvement in MB removal was observed when the agitation speed increased from 0 to 100 rpm, with efficiency rising from 40.07% to 99.39%. The enhancement can be ascribed to the

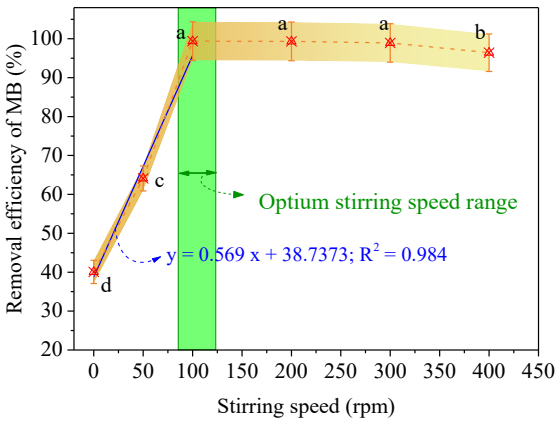

Fig 9. Influence of stirring speed on the removal performance of AHC for MB.

improved convective transport at the solid–liquid interface, which reduces the boundary layer resistance and promotes diffusion of MB molecules to active sites on the adsorbent surface. Further increases from 100 to 200 rpm showed negligible changes in removal efficiency (up to 99.33%), suggesting that mass transfer resistance was no longer rate-limiting. However, a slight decline in performance was observed at higher speeds (98.94% at 300 rpm and 96.42% at 400 rpm), likely due to increased mechanical shear disrupting adsorbate–adsorbent interactions or reducing effective contact time, leading to partial desorption. Based on these findings, a stirring speed of 100 rpm was identified as optimal, balancing adsorption efficiency with operational energy demands.

b. Effect of pH

The adsorption performance of MB on AHC was strongly governed by the solution pH. In this study, pH was varied from 3 to 11, while other experimental conditions initial MB 100 mg/L, 30 °C, time 180 min, and stirring speed (100 rpm) were held constant (Fig. 10). MB removal efficiency increased notably from 52.93% to a maximum of 99.73% as pH increased from acidic to near-neutral values, peaking at pH = 8. At low pH (3 – 4), the AHC surface becomes protonated, reducing electrostatic attraction between the positively charged MB molecules and the adsorbent. Additionally, excessive hydronium ions (H_3O^+) compete with MB for active sites, resulting in suppressed adsorption (Tran *et al.*, 2022). As the pH rises to 6–8, the surface acquires more negative charge, enhancing electrostatic interactions with MB and achieving nearly complete removal. Beyond pH = 8, a slight decline in efficiency was observed, though values remained consistently above 98%. This reduction may be attributed to site saturation or changes in surface chemistry under strongly alkaline conditions. Based on these results, a neutral pH (pH = 7) was chosen for further studies due to its favorable combination of adsorption efficiency and chemical stability, as well as the advantage of requiring no pH modification, which is beneficial for practical wastewater treatment applications (Tran *et al.*, 2022).

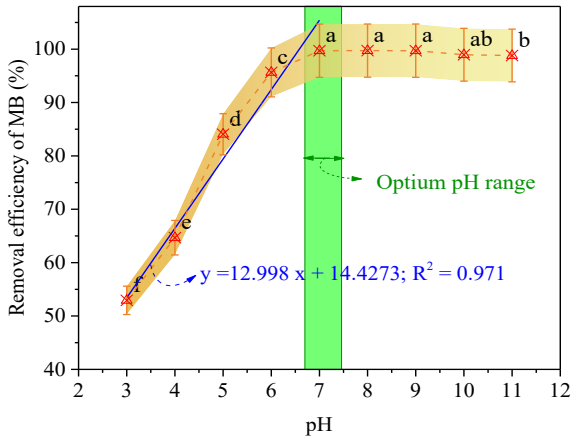

Fig 10. Effect of pH on MB removal by AHC.

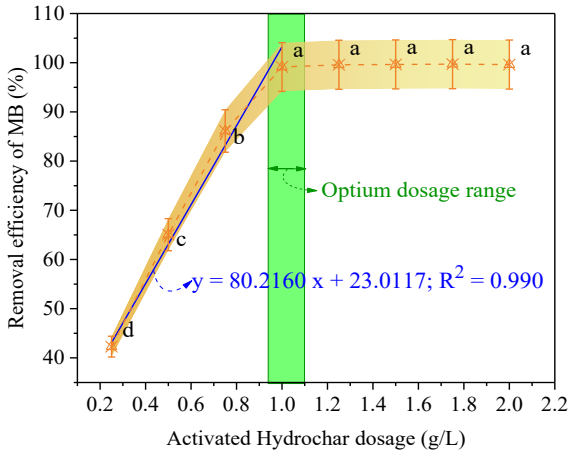

Fig 11. The effect of AHC adsorbent's dosage.

c. Effect of the dosage of AHC adsorbent

The influence of AHC dosage on the adsorption performance of MB was assessed by varying the adsorbent concentration from 0.25 to 2.00 g/L, while other experimental conditions, initial MB 100 mg/L, pH = 7, 30 °C, time 180 min, and stirring speed (100 rpm) were held constant (Fig. 11). As shown in the results, MB removal efficiency increased markedly from 42.28% to 99.13% when the dosage was raised from 0.25 to 1.00 g/L, primarily due to the greater availability of surface-active sites and adsorptive area. Beyond 1.0 g/L dosage, efficiency plateaued (up to 99.71%), indicating a saturation threshold. This trend may result from adsorbent agglomeration at elevated dosages, which reduces the effective surface area accessible for dye molecules. Furthermore, with the dye concentration fixed, the number of available MB molecules becomes limiting; thus, additional adsorbent mass offers negligible improvement (Tran *et al.*, 2022). Hence, 1.0 g/L of AHC was considered to be optimal for MB adsorption efficiency, it was selected for subsequent experiments.

d. Effect of C_o and contact duration on MB removal by AHC

The influence of initial MB concentration and contact time on its adsorption onto AHC was systematically examined under controlled conditions (pH = 7, 30 °C, 100 rpm, 1.0 g/L adsorbent dosage). A series of batch experiments were conducted with initial MB concentrations ranging from 50 to 500 mg/L over a 16-hour period (Fig. 12). The time required to attain adsorption equilibrium was markedly influenced by the initial MB concentration on AHC. At low concentrations (50 and 100 mg/L), equilibrium was rapidly reached within 20 minutes,

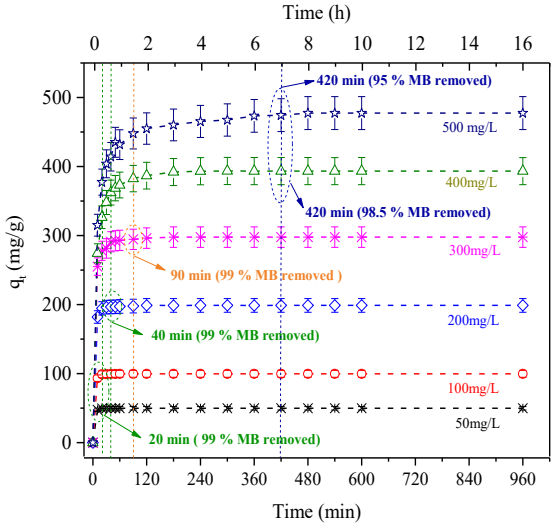

Fig 12. Effect of initial MB concentration and adsorption time on MB removal efficiency onto AHC

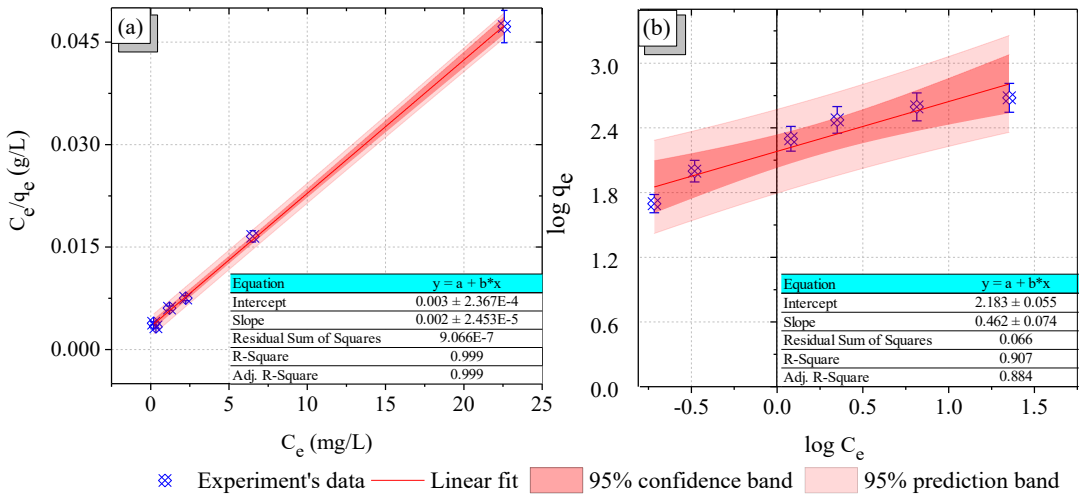

Fig 13. Linearized plots of (a) Langmuir and (b) Freundlich isotherm models

achieving ~99% removal efficiency. As the initial dye concentrations were raised to 200 and 300 mg/L, the time required to reach adsorption equilibrium increased to 40 and 90 minutes, respectively. These values were significantly shorter than those observed in previous studies using similar coffee husk-derived adsorbents, including AH and KOH-modified variants (Tran *et al.*, 2020, Tran *et al.*, 2021).

At elevated initial concentrations of 400 and 500 mg/L, the adsorption process exhibited a substantial prolongation in the time required to achieve maximum removal efficiency, reaching up to 420 minutes. This extended equilibration can be attributed to intensified competition for active sites and reduced diffusion efficiency within the microporous structure of AHC. In contrast, under low-concentration conditions, a greater proportion of adsorption sites remained accessible, enabling faster dye adsorption (Tran *et al.*, 2022). The observed trend underscores the role of mass transfer resistance in limiting adsorption kinetics at high pollutant loads and highlights the importance of optimizing contact time according to the initial solute concentration for efficient system design (Tran *et al.*, 2022).

3.3.2 Equilibrium studies

Adsorption isotherm models serve as a fundamental tool to elucidate the equilibrium relationship between adsorbates and the surface of adsorbents, offering critical insights for the design and optimization of large-scale adsorption systems (Tran *et al.*, 2022). These models describe how adsorbate molecules distribute between the liquid phase and the solid surface of AHC at equilibrium conditions. The fitting of experimental data to various isotherm models enables the identification of the most representative mechanism, thereby facilitating accurate system modeling and scale-up. This analysis provided insight into which model best describes the adsorption mechanism and aids in predicting system performance under practical environmental conditions (Tran *et al.*, 2022). In this work, the adsorption characteristics of the synthesized AHC were analyzed using two widely employed isotherm models, Langmuir and Freundlich. The degree of model fitting was assessed using the coefficient of determination (R^2), calculated from the linearized forms of the respective isotherm equations (Tran *et al.*, 2022). For the Langmuir model, the maximum adsorption capacity (Q_m) and the Langmuir constant (K_L) were calculated from the slope and intercept of the linear plot of C_e/q_e against C_e (Fig. 13a). The resulting adsorption parameters are summarized in Table 2.

Table 2
Adsorption isotherms for MB adsorbed onto the AHC

The isotherm model	Parameters	AHC this study	ACHC-KOH 1M (Tran *et al.*, 2021)
Langmuir	Q_m	499.48 ± 36.016	357.14
	K_L	1.611 ± 0.201	0.6667
	R_L	0.0012 - 0.0123	0.0030 - 0.0291
	R^2	0.987	0.9998
Freundlich	K_F	138.635 ± 18.103	129.60
	n	2.148 ± 0.300	4.1000
	R^2	0.864	0.6612
$q_{experiment}$	q_{exp}	477.43 ± 0.0124	357.38 ± 0.3485

In the case of the Freundlich model, the constants K_F and 1/n were derived from the slope and intercept of the log–log plot of q_e versus C_e (Fig. 13b). Values of 1/n ranging from 0 to 1 indicate that adsorption proceeds under favorable conditions. The corresponding Freundlich parameters are also listed in Table 2. The fitting accuracy of the Langmuir and Freundlich models was examined through comparison with experimental

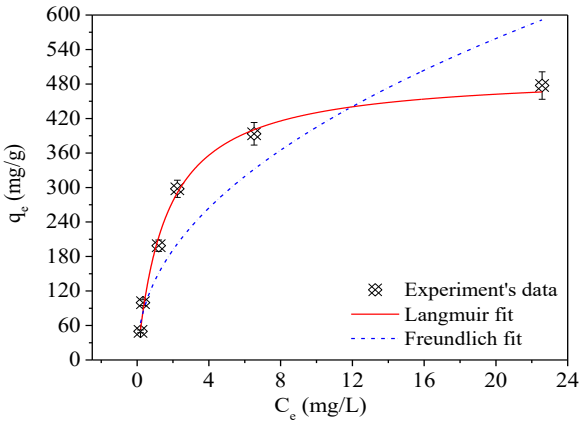

Fig 14. Linearized fitting of MB adsorption onto AHC using Langmuir, Freundlich models.

Table 3
Maximum MB adsorption capacities of biomass-derived carbonaceous adsorbents prepared via KOH activation under various synthesis conditions

Activated carbons	Method	Activator	BET (m^2/g)	Q_m (mg/g)	Isotherm model	References
Coffee husks (AHC)	One-step HTC, pyrolysis 700°C	KOH 1M	1022.3	499.5	Langmuir	This study
Corncob (AHC-KOH)	Two-step HTC, pyrolysis 800°C	KOH 1M	965.0	498.4	Langmuir	(Tran *et al.*, 2022)
Coffee husks (AH)	Two-step HTC, pyrolysis 800°C	KOH 1M	862.2	416.7	Langmuir	(Tran *et al.*, 2020)
Coffee husks (ACHC-KOH 1 M)	Two-step HTC, pyrolysis 700°C	KOH 1M	703.9	357.4	Langmuir	(Tran *et al.*, 2021)
Coffee husks (ACHC-KOH 1:1)	Two-step HTC, pyrolysis 700°C	Hydrochar : KOH (1:1)	743.8	316.5	Langmuir	(Tran *et al.*, 2021)
Corncobs	Pyrolysis 700°C and microwave 600 W	KOH (ratio 1.75)	492.0	333.0	Langmuir	(Medhat *et al.*, 2021)
Sugarcane bagasse waste (SBW)	Pyrolysis 700°C	SBW : KOH (1:2)	709.3	136.5	Freundlich	(Jawad *et al.*, 2021)
Bamboo (KBBC-900)	Two-step pyrolysis	KOH 3M	562	67.5	Langmuir	(Ge *et al.*, 2023)

MB adsorption data onto AHC (Fig. 14). Specifically, the Langmuir model exhibited an excellent correlation with the experimental data, characterized by a high coefficient of determination (R^2 = 0.987) in Table 2. This suggests that the adsorption process is predominantly monolayer in nature and occurs on a homogeneous surface with energetically equivalent active sites. The theoretical maximum adsorption capacity (q_m) derived from the Langmuir model was 499.48 ± 36.016 mg/g, closely aligning with the experimentally observed value (q_{exp} = 477.43 ± 0.0124 mg/g), further confirming the suitability of this model. Moreover, the dimensionless separation factor (R_L), calculated for initial dye concentrations of 50 and 500 mg/L, yielded values of 0.0123 and 0.0012, respectively, indicating a highly favorable adsorption process ($0 < R_L < 1$).

In contrast, the Freundlich model provided a relatively poorer fit to the data, with an R^2 value of 0.907, suggesting that it may be less appropriate in describing the adsorption mechanism under the studied conditions. Although the Freundlich constant (K_F = 138.635 $(mg/g(L/mg)^{1/n})$ indicates a substantial adsorption capacity and the adsorption intensity parameter (n = 2.148) reflects a favorable adsorption process (n > 1), the overall statistical performance of the model was inferior to that of the Langmuir isotherm. Therefore, it can be inferred that the adsorption of methylene blue onto AHC is best described by the Langmuir model, implying a monolayer adsorption process on a structurally and energetically uniform surface (Cao *et al.*, 2014, Tran *et al.*, 2020). In this work, the one-step HTC-produced AHC exhibited a maximum methylene blue adsorption capacity (Q_m = 499.48 mg/g), which was notably higher than that of the two-step HTC-derived AHC-KOH 1 M (Q_m = 357.14 mg/g) synthesized from the same coffee husk precursor reported in the authors' earlier study (Tran *et al.*, 2021). This improvement may be related to the larger specific surface area of AHC than AHC-KOH 1 M (Δ_{BET} = 318.46 m^2/g). Although the overall surface functionalities of oxygenated AHC were slightly lower than those of two-step AHC-KOH 1M (Table 1), together with the larger proportion of lactone groups, it could promote stronger interactions with cationic dye molecules via π–π electron-donating and hydrogen-bonding mechanisms, thus compensating for the slight decrease of carboxylic and phenolic groups in adsorption performance. The results of the study showed that not only did it save time and reduce heat, but it also had a superior MB adsorption capacity compared to the traditional two-step HTC method, as well as the conventional two-step pyrolysis or microwave-coupled pyrolysis presented in Table 3. This demonstrated the potential of one-step HTC as a sustainable strategy to enhance the value of coffee husks in particular and waste biomass in general into high-performance adsorbents, which can be applied in sustainable water treatment.

3.3.3 Adsorption kinetics

Kinetic parameters derived from the models and their corresponding experimental data are shown in Fig. 15 and summarized in Table 4. The PFO model showed limited model–experiment agreement, suggesting that it does not sufficiently capture the adsorption dynamics of MB onto AHC. The adsorption kinetics of MB onto AHC were comprehensively analyzed using the PFO and PSO kinetic models (Fig. 15). These models were applied to interpret the time-dependent adsorption profiles and to elucidate the dominant adsorption mechanism. As summarized in Table 4, the PFO model exhibited only moderate correlation coefficients (R^2 = 0.855 – 0.955) and substantial discrepancies between the experimental (q_{exp}) and calculated ($q_{e,cal}$) adsorption capacities, particularly at higher initial MB concentrations. For instance, at 500 mg/L, the q_{exp} was 477.43 mg/g, whereas the $q_{e,cal}$ predicted by the PFO model was significantly lower (92.95 mg/g), indicating limited model applicability under these conditions. Hence, the adsorption behavior of MB onto AHC could not be satisfactorily described by the PFO kinetic framework.

Conversely, the PSO model provided an excellent fit to the experimental data, with correlation coefficients consistently approaching unity ($R^2 \geq 0.9999$) across all concentrations examined. The calculated and experimental qe values were closely matched, for example, at 500 mg/L, q_{exp} and $q_{e,cal}$ were 477.43 and 476.19 mg/g, respectively. Moreover, the corresponding sum of squared error (SSE determined from Eq.10 values for the PSO model remained below 1% in most cases, confirming its superior predictive reliability. The relatively high initial adsorption rate (h), determined from Eq. 9, particularly at low to intermediate MB concentrations, suggests that the early stage of adsorption is governed by strong chemical interactions between MB molecules and the surface functional groups of AHC.

Overall, the PSO model more accurately represents the MB adsorption kinetics on AHC. PSO kinetics indicate that the rate-

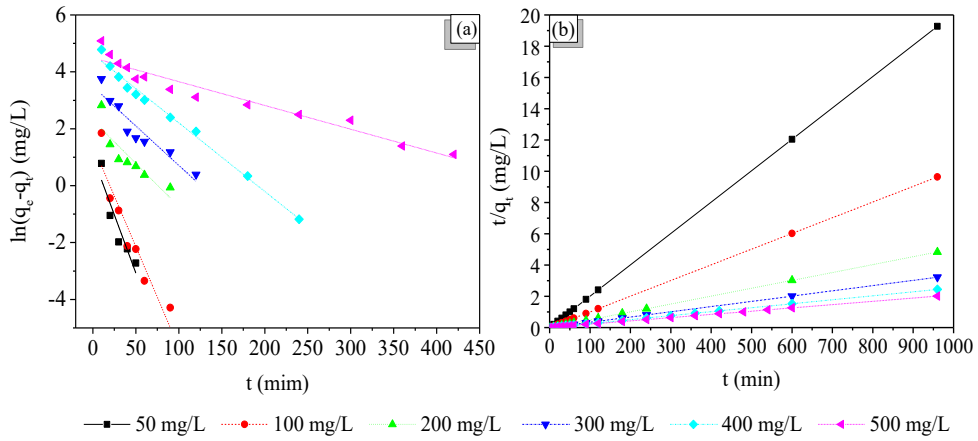

Fig 15. Linearized kinetics of MB adsorption onto AHC: (a) PFO, (b) PSO.

Table 4
Kinetic parameters for MB adsorption onto AHC (PFO and PSO models)

MB (mg/L)	q_{exp} (mg/g)	PFO				PSO				
		$q_{e,cal}$	R^2	k_1	SSE_1	$q_{e,cal}$	k_2	R^2	h	SSE_2
50	49.81	2.77	0.8761	0.0818	27.16	47.85	0.0196	1.0000	44.843	1.1321
100	99.67	4.10	0.8889	0.0711	55.18	99.01	0.0567	1.0000	555.556	0.3809
200	198.80	12.94	0.8550	0.0345	107.31	200.00	0.0156	1.0000	625.000	0.6944
300	297.76	24.03	0.8575	0.0206	158.04	294.12	0.0036	1.0000	312.500	2.1031
400	393.48	70.21	0.9305	0.0181	186.64	400.00	0.0009	1.0000	147.059	3.7645
500	477.43	92.95	0.9546	0.0088	221.98	476.19	0.0004	0.9999	84.746	0.7133

limiting step of MB adsorption is governed by surface chemical bonding rather than mass transfer or external diffusion. This suggests that adsorption occurs predominantly through valence forces arising from ion exchange, π–π interactions, or electrostatic attraction between the cationic dye and negatively charged functional sites on the hydrochar (Ge *et al.*, 2023). The strong correlation also implies that the number of active sites remains constant during the reaction, with equilibrium being reached when these sites are fully occupied, consistent with chemisorption-controlled kinetics. The results are consistent with those of material synthesized by the 2-step HTC method from the same coffee husk precursor reported in the authors' previous study (Tran *et al.*, 2021, Tran *et al.*, 2020), yet this work distinguishes itself by delivering similar adsorption efficiency through a faster and more energy-efficient preparation route.

3.4 Reusability assessment of AHC based on MB adsorption performance.

The regeneration efficiency of AHC was systematically assessed across six successive adsorption–desorption runs, as shown in Fig. 16. A noticeable reduction in MB removal efficiency was observed after repeated use. In the first adsorption cycle, the AHC material exhibited an outstanding removal efficiency of 99.67%. However, subsequent cycles showed a progressive reduction in performance, with adsorption yields decreasing to 80.36%, 67.82%, 52.75%, 50.41%, and 48.29% after the second through sixth regenerations, respectively. The decreasing trend in MB removal is closely correlated with a concomitant decline in the total surface acidity of AHC, as indicated by the reduction in total acid concentration (1.803 to 0.481 mmol/g) across cycles. The loss of acidic functional groups, which govern electrostatic and π–π interactions with MB, may explain the diminishing adsorption capacity upon regeneration. This

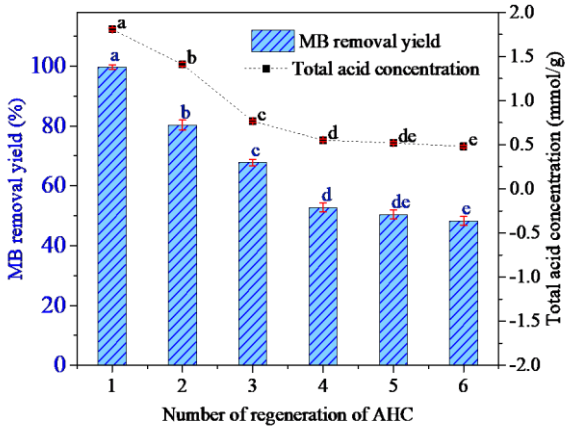

Fig 16. Illustrates the reusability of AHC through multiple adsorption–desorption cycles; different letters indicate significance (Tukey HSD, $p < 0.05$).

observation suggests partial degradation or leaching of surface-active sites during the regeneration protocol, despite the mild desorption conditions employed. Statistical analysis (as denoted by different superscript letters above the bars in Fig. 14) confirmed significant differences in adsorption performance among cycles ($p < 0.05$), particularly after the third regeneration. Nevertheless, the material maintained more than 50% adsorption performance following five successive regeneration cycles, indicating a moderate level of reusability suitable for practical wastewater treatment applications.

These results reaffirm the significance of maintaining surface functionality upon regeneration and concur with earlier

reports on activated carbons (Pathania *et al.*, 2017, Tran *et al.*, 2021, Tran *et al.*, 2022, Ge *et al.*, 2023), and further highlight that comparable adsorption performance can be attained via our one-step hydrothermal route, which significantly reduces both synthesis duration and thermal energy consumption.

4. Conclusion

Activated hydrochar was successfully synthesized from coffee husk through a one-step HTC in the presence of KOH under mild temperature conditions. The resulting material has a large surface area and a high density of oxygen-containing functional groups (1.806 mmol/g), which contributed to its excellent adsorption performance. The AHC exhibited an effective MB adsorption capacity of 95.48% (477.43 mg/g). The adsorption process followed a chemical adsorption mechanism, showing excellent agreement with the Langmuir isotherm and PSO kinetic model. In addition, AHC material maintained more than 50% of its original adsorption capacity after five successive reuse cycles, indicating a satisfactory level of regeneration stability. These results underscore AHC's promise as an eco-efficient material capable of eliminating cationic dyes in aqueous systems, thereby promoting biomass valorization and environmentally benign wastewater treatment.

Acknowledgements

The author gratefully acknowledges the support from the Industrial University of Ho Chi Minh City.

Author Contributions: Thi Hien Tran: Conceptualization, methodology, formal analysis, writing-original draft, supervision, resources, writing-review and editing, project administration, validation. The author has read and agreed to the published version of the manuscript.

Funding: The author received no financial support for the research, authorship, and/or publication of this article.

Conflicts of Interest: The author declares no conflict of interest.

Reference

Akbari, A., Peighambardoust, S. J. & Kazemian, H. (2025). Comparative study on the impact of physicochemical characteristics of the activated carbons derived from biochar/hydrochar on the adsorption performances of article. *Environ Res.* 270 121022. https://doi.org/10.1016/j.envres.2025.121022

Bielecki, M. & Zubkova, V. (2023). Analysis of Interactions Occurring during the Pyrolysis of Lignocellulosic Biomass of article. *Molecules.* 28 (2), 506. https://doi.org/10.3390/molecules28020506

Cao, J. S., Lin, J. X., Fang, F., Zhang, M. T. & Hu, Z. R. (2014). A new absorbent by modifying walnut shell for the removal of anionic dye: Kinetic and thermodynamic studies of article. *Bioresour Technol.* 163 199-205. http://dx.doi.org/10.1016/j.biortech.2014.04.046

De Benedicto, D. F. C., Ferreira, G. M. D. & Thomasi, S. S. (2024). β-cyclodextrin-functionalized coffee husk biochar for surfactant adsorption of article. *Colloids Surf A Physicochem Eng Asp.* 701 134921. https://doi.org/10.1016/j.colsurfa.2024.134921

Ge, Q., Li, P., Liu, M., Xiao, G.-M., Xiao, Z.-Q., Mao, J.-W. & Gai, X.-K. (2023). Removal of methylene blue by porous biochar obtained by KOH activation from bamboo biochar of article. *Bioresour Bioproc.* 10 (1), 51. https://doi.org/10.1186/s40643-023-00671-2

Gil-Muñoz, G., Benguella, S. & Alcañiz-Monge, J. (2025). Impact of hydrothermal treatment and activation atmosphere on the porosity development of activated carbon from date pits of article. *Fuel Process Technol.* 276 108264. https://doi.org/10.1016/j.fuproc.2025.108264

Gong, M., Xu, F., Liu, P., Xu, Q., Su, Y., Fan, Y. & Li, M. (2025). A review of biomass hydrochar as an adsorbent: Performance, modification, and applications of article. *J. Water Process Eng.* 71 107314. https://doi.org/10.1016/j.jwpe.2025.107314

Hendronursito, Y., Astuti, W., Sabarman, H. & Santoso, I. (2025). A porous activated carbon derived from banana peel by hydrothermal activation two-step methods of article. *Int. J. Renew. Energy Dev.* 14 (2), 10. https://doi.org/10.61435/ijred.2025.60847

Hussein, S. A. & Ahmed, M. J. (2026). Batch and fixed-bed adsorption of phosphate and nitrate on char derived by the co-pyrolysis of waste tires and corn cobs of article. *Int. J. Renew. Energy Dev.* 15 (1), 15. https://doi.org/10.61435/ijred.2026.61629

Illingworth, J. M., Rand, B. & Williams, P. T. (2022). Understanding the mechanism of two-step, pyrolysis-alkali chemical activation of fibrous biomass for the production of activated carbon fibre matting of article. *Fuel Process Technol.* 235 107348. https://doi.org/10.1016/j.fuproc.2022.107348

Indexbox. (2024). *World - Synthetic Organic Coloring Matter And Pigments - Market Analysis, Forecast, Size, Trends and Insights* https://www.indexbox.io/blog/organic-pigments-world-market-overview-2024-6/ Accessed Sep 1, 2025.

Jain, A., Balasubramanian, R. & Srinivasan, M. P. (2016). Hydrothermal conversion of biomass waste to activated carbon with high porosity: A review of article. *Chem Eng J.* 283 789-805. http://dx.doi.org/10.1016/j.cej.2015.08.014

Jalilian, M., Bissessur, R., Ahmed, M., Hsiao, A., He, Q. S. & Hu, Y. (2024). A review: Hydrochar as potential adsorbents for wastewater treatment and CO_2 adsorption of article. *Sci Total Environ.* 914 169823. https://doi.org/10.1016/j.scitotenv.2023.169823

Jawad, A. H., Abdulhameed, A. S., Bahrudin, N. N., Hum, N., Surip, S. N., Syed-Hassan, S. S. A., Yousif, E. & Sabar, S. (2021). Microporous activated carbon developed from KOH activated biomass waste: surface mechanistic study of methylene blue dye adsorption of article. *Water Sci. Technol.* 84 (8), 1858-1872. https://doi.org/10.2166/wst.2021.355

Jerzak, W., Acha, E. & Li, B. (2024). Comprehensive Review of Biomass Pyrolysis: Conventional and Advanced Technologies, Reactor Designs, Product Compositions and Yields, and Techno-Economic Analysis of article. *Energies.* 17 (20), 5082. https://doi.org/10.3390/en17205082

Khruengsai, S., Pripdeevech, P., Pongnailert, S., Chanlek, N., Thumanu, K., Muangmora, R., Rojviroon, T. & Pongpiachan, S. (2024). Chemical characterization of activated carbon derived from Napier grass, rubber wood, bamboo, and hemp of article. *Int. J. Renew. Energy Dev.* 13 (6), 10. https://doi.org/10.61435/ijred.2024.60502

Krishna Murthy, T. P., Gowrishankar, B. S., Krishna, R. H., Chandraprabha, M. N. & Mathew, B. B. (2020). Magnetic modification of coffee husk hydrochar for adsorptive removal of methylene blue: Isotherms, kinetics and thermodynamic studies of article. *Environ Chem Ecotoxicol.* 2 205-212. https://doi.org/10.1016/j.enceco.2020.10.002

Liu, P., Sun, S., Huang, S., Wu, Y., Li, X., Wei, X. & Wu, S. (2024). KOH activation mechanism in the preparation of Brewer's spent grain-based activated carbons of article. *Catalysts.* 14 (11), 814. https://doi.org/10.3390/catal14110814

Luo, Y., Lan, Y., Liang, S., Yu, S., Xue, M., Yin, Z., Shen, F.-F., Li, X., Hong, Z., Yan, M., Xie, C. & Gao, B. (2024). Rice husk hydrochar prepared by hydrochloric acid assisted hydrothermal carbonization for levofloxacin removal in bioretention columns of article. *Bioresour Technol.* 393 130105. https://doi.org/10.1016/j.biortech.2023.130105

Medhat, A., El-Maghrabi, H. H., Abdelghany, A., Abdel Menem, N. M., Raynaud, P., Moustafa, Y. M., Elsayed, M. A. & Nada, A. A. (2021). Efficiently activated carbons from corn cob for methylene blue adsorption of article. *Appl Surf Sci Adv.* 3 100037. https://doi.org/10.1016/j.apsadv.2020.100037

Nandi, R., Jha, M. K., Guchhait, S. K., Sutradhar, D. & Yadav, S. (2023). Impact of KOH activation on rice husk derived porous activated carbon for carbon capture at flue gas alike temperatures with high CO_2/N_2 Selectivity of article. *ACS Omega.* 8 (5), 4802-4812. https://doi.org/10.1021/acsomega.2c06955

Pathania, D., Sharma, S. & Singh, P. (2017). Removal of methylene blue by adsorption onto activated carbon developed from Ficus carica bast of article. *Arab J Chem.* 10 S1445-S1451. https://doi.org/10.1016/j.arabjc.2013.04.021

Polaert, I., Estel, L., Huyghe, R. & Thomas, M. (2010). Adsorbents regeneration under microwave irradiation for dehydration and volatile organic compounds gas treatment of article. *Chem Eng J*. 162 (3), 941-948. https://doi.org/10.1016/j.cej.2010.06.047

Rocha, L. S., Pereira, D., Sousa, É., Otero, M., Esteves, V. I. & Calisto, V. (2020). Recent advances on the development and application of magnetic activated carbon and char for the removal of pharmaceutical compounds from waters: A review of article. *Sci Total Environ*. 718 137272. https://doi.org/10.1016/j.scitotenv.2020.137272

Rubinstein, A. (2024). USDA Attache: Vietnam's 2024 Coffee Crop Revised Up to 30.1 Million Bags; https://www.stonex.com/en/market-intelligence/coffee/202412091837/usda-attache-vietnams-2024-coffee-crop-revised-up-to-301-millio/ Accessed Dec 9, 2024.

Rustamaji, H., Prakoso, T., Devianto, H., Widiatmoko, P., Febriyanto, P., Ginting, S. B. & Darmansyah, D. (2025). Synthesis of rubber seed shell-derived porous activated carbons for promising supercapacitor application of article. *Int. J. Renew. Energy Dev*. 14 (2), 11. https://doi.org/10.61435/ijred.2025.60869

Rustamaji, H., Prakoso, T., Rizkiana, J., Devianto, H., Widiatmoko, P. & Guan, G. (2022). Synthesis and Characterization of Hydrochar and Bio-oil from Hydrothermal Carbonization of Sargassum sp. using Choline Chloride (ChCl) Catalyst of article. *Int. J. Renew. Energy Dev*. 11 (2), 10. https://doi.org/10.14710/ijred.2022.42595

Saha, N., Volpe, M., Fiori, L., Volpe, R., Messineo, A. & Reza, M. T. (2020). Cationic dye adsorption on hydrochars of winery and citrus juice industries residues: Performance, mechanism, and thermodynamics of article. *Energies*. 13 (18), 4686. https://doi.org/10.3390/en13184686

Selvam, S. M., Janakiraman, T. & Paramasivan, B. (2021). Characterization of engineered corn cob biochar produced in allothermal pyrolysis reactor of article. *Mater Today Proc*. 47 312-317. https://doi.org/10.1016/j.matpr.2021.04.469

Selvaraj, P. S., Ettiyagounder, P., Sabarish, K., Periasamy, K., Rengasamy, B., Veeraswamy, D., Karchiyappan, T. & Kathirvel, S. (2025). Hydrothermal carbonization approach for transforming biomass waste to value added hydrochar and its applications in water remediation of article. *Desalin Water Treat*. 322 101199. https://doi.org/10.1016/j.dwt.2025.101199

Service, U. F. A. (2025). Usda biannual report lowers its estimate of world production for 2024/25 to 174.4 million, global output at 178.7 million in 2025/26. https://www.comunicaffe.com/usda-biannual-report-cuts-estimate-of-world-production-for-2024-25-to-174-4-million/ Accessed June 26, 2025.

Tamilselvan, K., Sundarajan, S., Ramakrishna, S., Amirul, A.-a. A. & Vigneswari, S. (2024). Sustainable valorisation of coffee husk into value added product in the context of circular bioeconomy: Exploring potential biomass-based value webs of article. *Food and Bioproducts Processing*. 145 187-202. https://doi.org/10.1016/j.fbp.2024.03.008

Tran, T. H., Le, A. H., Pham, T. H., Duong, L. D., Nguyen, X. C., Nadda, A. K., Chang, S. W., Chung, W., Nguyen, D. D. & Nguyen, D. T. (2022). A sustainable, low-cost carbonaceous hydrochar adsorbent for methylene blue adsorption derived from corncobs of article. *Environ Res*. 113178. https://doi.org/10.1016/j.envres.2022.113178

Tran, T. H., Le, A. H., Pham, T. H., Nguyen, D. T., Chang, S. W., Chung, W. J. & Nguyen, D. D. (2020). Adsorption isotherms and kinetic modeling of methylene blue dye onto a carbonaceous hydrochar adsorbent derived from coffee husk waste of article. *Sci Total Environ*. 725 138325. https://doi.org/10.1016/j.scitotenv.2020.138325

Tran, T. H., Le, H. H., Pham, T. H., Nguyen, D. T., La, D. D., Chang, S. W., Lee, S. M., Chung, W. J. & Nguyen, D. D. (2021). Comparative study on methylene blue adsorption behavior of coffee husk-derived activated carbon materials prepared using hydrothermal and soaking methods of article. *J Environ Chem Eng*. 9 (4), 105362. https://doi.org/10.1016/j.jece.2021.105362

Tran, T. H., Nguyen, T. V., Pham, H. T., Nguyen, D. T. & Phan, D. T. (2017). Synthesis of novel magnetic adsorbents from coffee husks by hydrothermal carbonization of article. *Vietnam Journal of Science and Technology*. 55 https://doi.org/10.15625/2525-2518/55/4/9016

Tran, T. H., Nguyen, T. V., Phan, T. Q. P., Pham, H. T., Nguyen, D. T. & Phan, D. T. (2016). Optimizing the process of transforming coffee husks into biochar by means of hydrothermal carbonization of article. *Journal of Science and Technology* 54 (4B), 138-145. https://doi.org/10.15625/2525-2518/54/4B/12034

Wei, T., Wei, X., Gao, Y. & Li, H. (2015). Large scale production of biomass-derived nitrogen-doped porous carbon materials for supercapacitors of article. *Electrochim Acta*. 169 186-194. http://dx.doi.org/10.1016/j.electacta.2015.04.082

Yang, Y., Foong, S. Y., He, Y., Liew, R. K., Ma, N. L., Yek, P. N. Y., Ge, S., Naushad, M. & Lam, S. S. (2024). Upcycling crab shell waste into biochar for treatment of palm oil mill effluent via microwave pyrolysis and activation of article. *Environ Res*. 248 118282. https://doi.org/10.1016/j.envres.2024.118282